Supporting Information for
Spin-locking in low frequency reaction yield detected magnetic resonance

by C. J. Wedge, Jason C. S. Lau, Kelly-Anne Ferguson, Stuart Norman, P. J. Hore and Christiane R. Timmel.

S0.1 Experimental details of RF field strength calibration

In order to allow continuous monitoring of the radiofrequency field strength B_1 a search loop was fixed close to the RF field coils and the induced voltage measured on an oscilloscope during all experiments. The fixed search loop was calibrated from a small search coil which could be inserted into the spectrometer in place of the sample cell. To produce the initial calibration a known field strength was required, which was produced using a small Helmholtz coil in a tuned circuit matched to the 50 Ω output of a frequency synthesiser. When driven at low powers to avoid heating effects the current in the coil was calculated from the input voltage using Ohm's law and the experimentally determined coil resistance at 36 MHz. Using the Biot-Savart law the field strength could then be calculated from the coil dimensions and current. To obtain the frequency dependent resistance of the calibration coil it was made to resonate with various known capacitances connected across the coil terminals. By measuring the Q of the resonant circuit the resistance could be found using,

$$R = \frac{1}{2\pi\nu_c CQ}. \tag{S1}$$

where ν_C is the resonant frequency for a capacitance C. Using capacitances in the range 15-65 pF the resonant frequency was varied from 32 to 51 MHz, and the coil resistance determined to be 0.92 Ω at 36 MHz.

A final correction to the measured RF field strengths is required due to the audiofrequency (AF) modulation of the RF field used to enable phase-sensitive detection. The mixing of the RF and AF signals is carried out using an AD835 4-quadrant multipler. Using the known functional form of the output function of this circuit, and by measuring with an oscilloscope the peak to peak voltage induced in the search coil and the minimum envelope height, it was possible to calculate the conversion from peak measured voltage to root mean square RF field strength.

S0.2 Additional RYDMR-B_0 spectra

Additional RYDMR-B_0 spectra for the orthogonal field arrangement are shown in Figure S1 for the Py-d_{10}/1,4-DCB system. Owing to the relatively small hyperfine coupling values on both radicals the hyperfine structure is well resolved for this system. For the other five systems studied to obtain B_1^0 data for Figure 4 the spectra are broader and very similar to the representative data shown in Figure 2, hence these data are not included here.

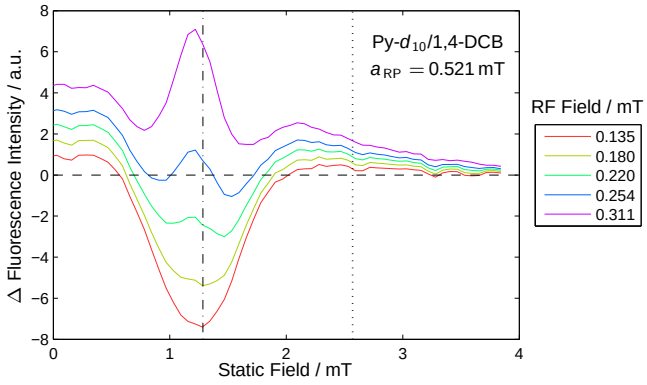

Figure S1: Experimental RYDMR-B_0 spectra of the Py-d_{10}/1,4-DCB system, for a 36 MHz oscillating field applied orthogonal to the static field. Vertical lines indicate the Larmor resonance field at 1.28 mT (dot-dashed line) and twice the Larmor resonance field at 2.56 mT (dotted line). The regularisation parameter λ was chosen to be 0.02 for this data set, owing to the smaller number of different B_1 values in comparison to the data in Figure 2 ($\lambda = 0.0005$).

S0.3 Experimental data for effect of Degenerate Electron Exchange on B_1^0

In order to investigate the effects of degenerate electron exchange RYDMR-B_1 spectra were collected for the Py-h_{10}/1,3-DCB system at various DCB concentrations. Figure S2 shows the resultant variation in the B_1^0 parameter which initially increases with DCB concentration in the slow exchange limit before reaching a maximum in the intermediate exchange regime. Experiments at higher concentrations were not possible due to insufficient solubility, but it is expected that a decrease to a plateau region would be observed as the fast exchange limit is entered [Justinek *et al.*, *J. Am. Chem. Soc.*, 2004, **126**, 5635].

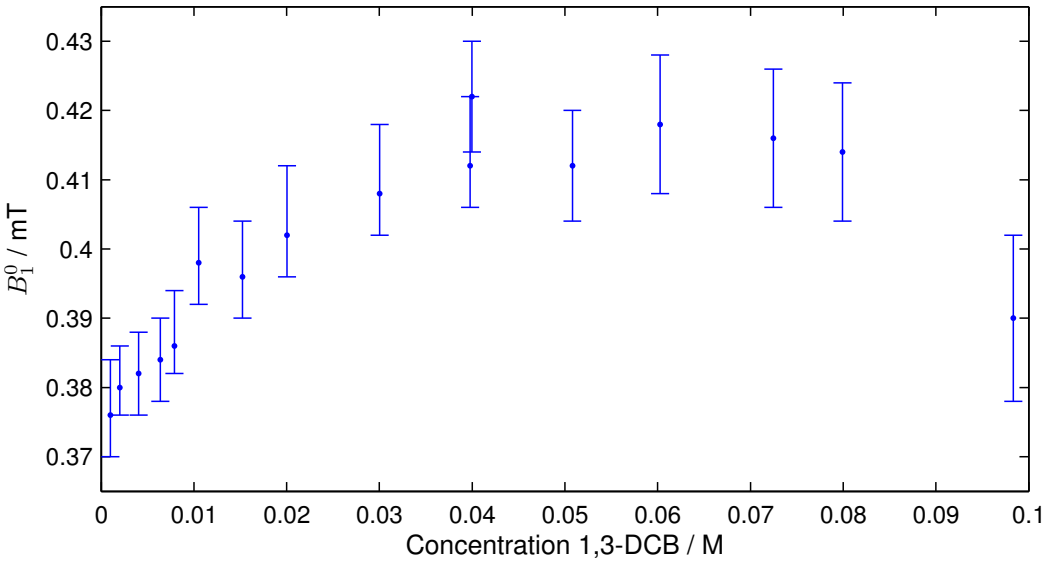

Figure S2: Variation in B_1^0 with DCB concentration for the Py-h_{10}/1,3-DCB system in 1:9 acetonitrile / cyclohexanol. Py-h_{10} 1.0 mM, $\nu_{rf} = 36$ MHz.

S0.4 Experimental data for orientation effects in RYDMR of micellar solutions

RYDMR-B_0 spectra for the Py-h_{10}/1,3-DCB system contained in two different sizes of alkylammonium chloride micelles are shown in Figure S3 for a range of RF field strenghts. There is a clear difference between the spectra in dodecyltrimethylammonium chloride (DTAC) and cetyltrimethylammonium chloride (CTAC), though this becomes less pronounced as B_1 is increased. Aside from the better resolved resonance effects in the $\theta = 90^\circ$ case for CTAC, the more subtle effect of the shift in the minima for the $\theta = 0^\circ$ case should be noted, this moving to higher static field strengths in the DTAC case. The broadening of the DTAC spectra as compared to the CTAC spectra suggests a shorter radical pair lifetime in the DTAC case (see paper for discussion) which is consistent with the smaller core volume of the micelle when using the shorter chain surfactant.

Simulations using γ-COMPUTE are presented in Figure S4, for two exponential model rate constants. No attempt has been made to fit the experimental data exactly (a more complex kinetic model including an additional rate for escape from the micelle would be required), simply to reproduce the general change in spectral features to show qualitatively that lifetime changes are apparent in the RYDMR spectra. It is clear that the broadening of the spectrum observed in the DTAC system compared to CTAC can be interpreted as arising from a reduction in radical pair lifetime. In the longer lifetime example (Figure S4, right column) the Zeeman resonance is observed for perpendicular orientation and low radiofrequency power, the resonance becoming less intense as B_1 is increased, as expected when moving from the spin-pumping to spin-locking regimes. By contrast in the shorter lived radical pair (Figure S4, left column) no obvious resonance effects are observed in the perpendicular case, and the broad signals begin to resemble some static effect of the oscillating field.

The experimental data were collected using 0.2 mM Py-h_{10} and 7.2 mM 1,3-DCB, these concentrations having been optimized to ensure that only one Py molecule is encapsulated per micelle. Simulations used the following hyperfine couplings: Py-$h_{10}^{\bullet+}$ $4\mathrm{H} \times 0.538\,\mathrm{mT}$, $4\mathrm{H} \times 0.212\,\mathrm{mT}$; $1,3\text{-DCB}^{\bullet-}$ $2\mathrm{H} \times 0.829\,\mathrm{mT}$, $1\mathrm{H} \times 0.144\,\mathrm{mT}$.

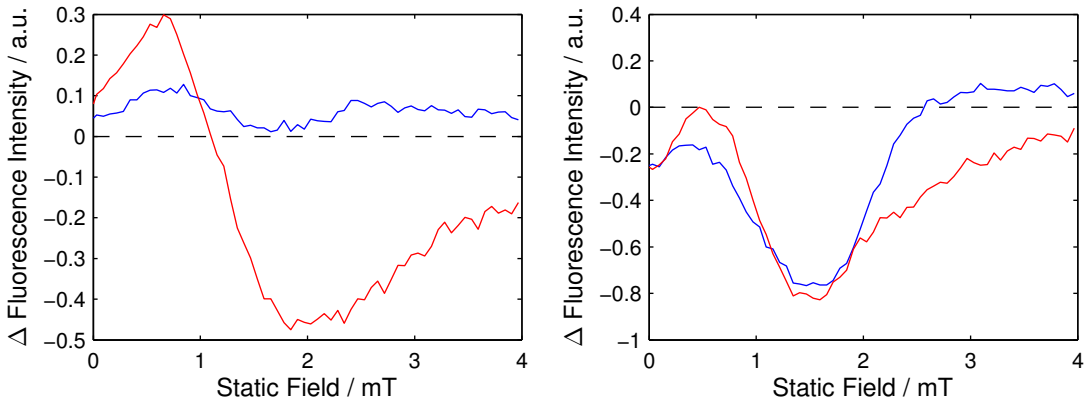

(a) DTAC, $B_1 \approx 0.24\,\mathrm{mT}$

(b) CTAC, $B_1 \approx 0.24\,\mathrm{mT}$

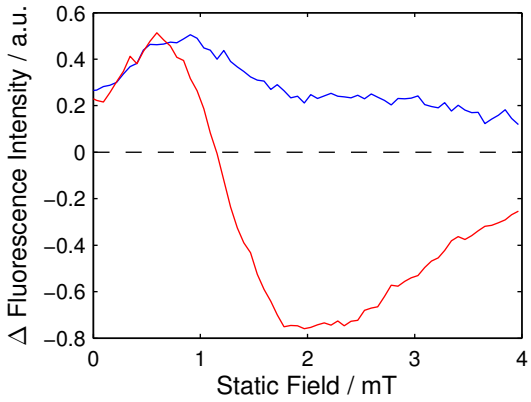

(c) DTAC, $B_1 \approx 0.3\,\mathrm{mT}$

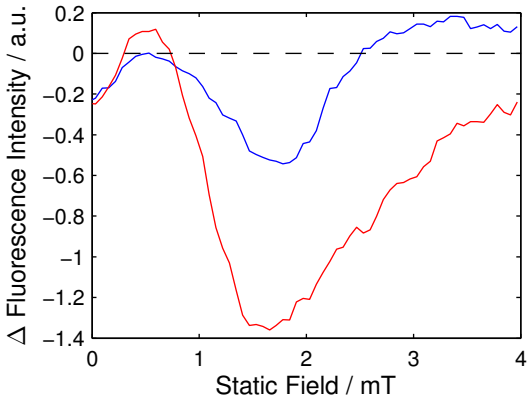

(d) CTAC, $B_1 \approx 0.32\,\mathrm{mT}$

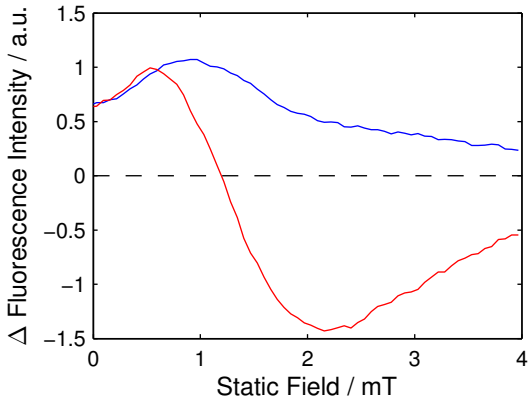

(e) DTAC, $B_1 \approx 0.40\,\mathrm{mT}$

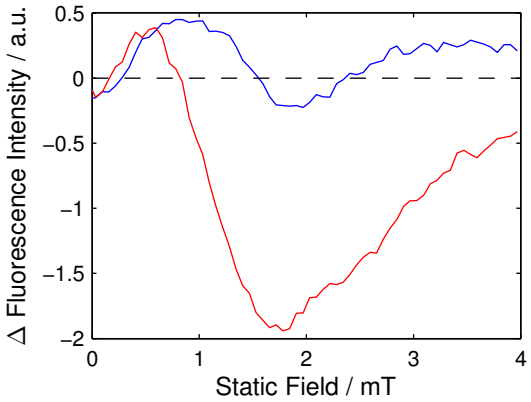

(f) CTAC, $B_1 \approx 0.38\,\mathrm{mT}$

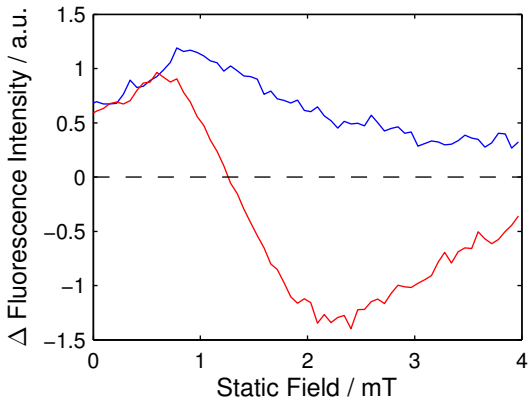

(g) DTAC, $B_1 \approx 0.50\,\mathrm{mT}$

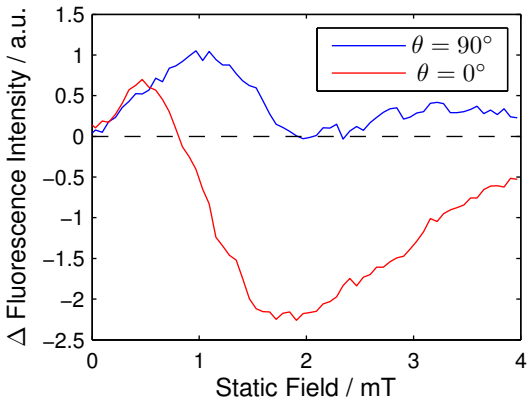

(h) CTAC, $B_1 \approx 0.52\,\mathrm{mT}$

Figure S3: RYDMR-B_0 spectra of the Py-h_{10}/1,3-DCB system comparing parallel and perpendicular orientations at different RF field strengths and for different micelles.

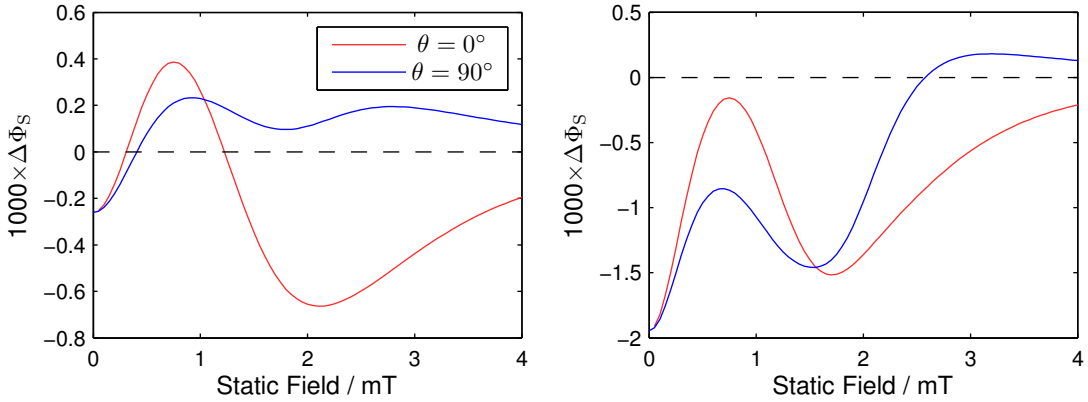

(a) $k = 1.6 \times 10^8\,\mathrm{s}^{-1}$, $B_1 = 0.2\,\mathrm{mT}$

(b) $k = 1.0 \times 10^8\,\mathrm{s}^{-1}$, $B_1 = 0.2\,\mathrm{mT}$

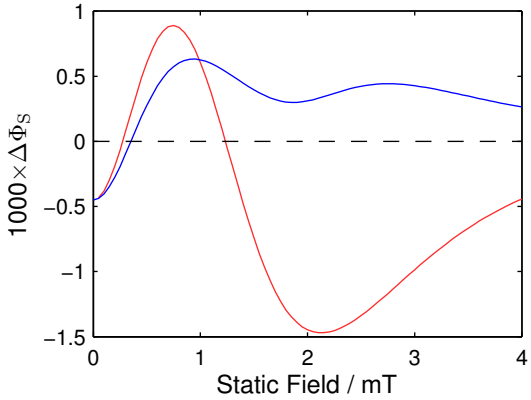

(c) $k = 1.6 \times 10^8\,\mathrm{s}^{-1}$, $B_1 = 0.3\,\mathrm{mT}$

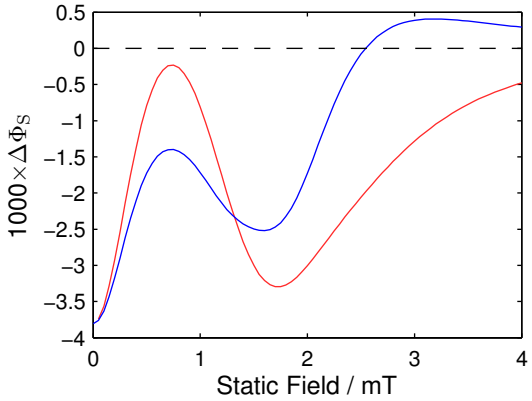

(d) $k = 1.0 \times 10^8\,\mathrm{s}^{-1}$, $B_1 = 0.3\,\mathrm{mT}$

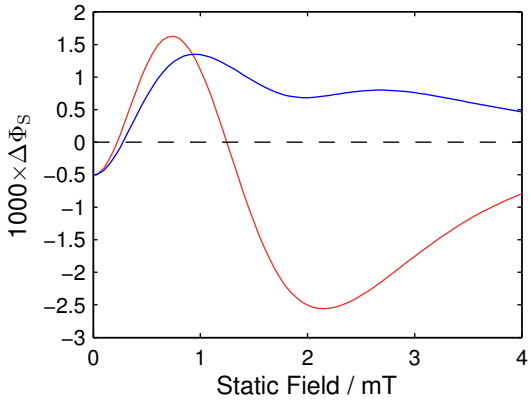

(e) $k = 1.6 \times 10^8\,\mathrm{s}^{-1}$, $B_1 = 0.4\,\mathrm{mT}$

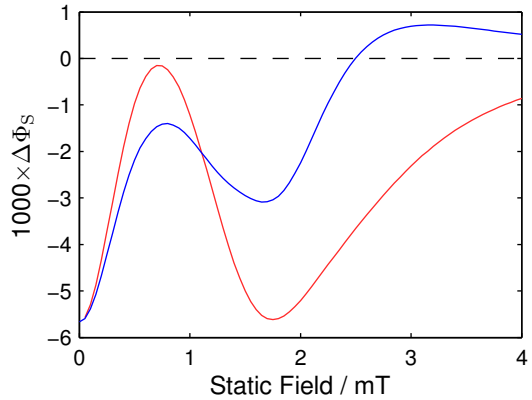

(f) $k = 1.0 \times 10^8\,\mathrm{s}^{-1}$, $B_1 = 0.4\,\mathrm{mT}$

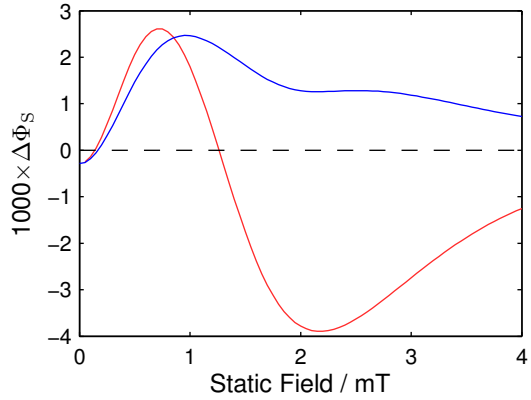

(g) $k = 1.6 \times 10^8\,\mathrm{s}^{-1}$, $B_1 = 0.5\,\mathrm{mT}$

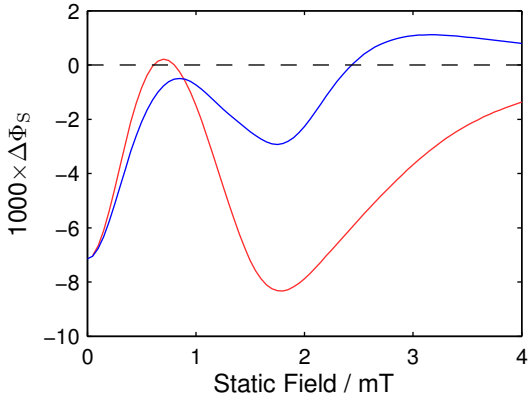

(h) $k = 1.0 \times 10^8\,\mathrm{s}^{-1}$, $B_1 = 0.5\,\mathrm{mT}$

Figure S4: γ-COMPUTE simulations of RYDMR-B_0 spectra of the Py-$h_{10}^{\bullet+}$/1,3-DCB$^{\bullet-}$ system comparing orientations for different RF field strengths and recombination rates.